ELSEVIER

International Journal of Solids and Structures 41 (2004) 2607–2621

INTERNATIONAL JOURNAL OF SOLIDS and STRUCTURES

www.elsevier.com/locate/ijsolstr

A fractional order rate approach for modeling concrete structures subjected to creep and fracture

F. Barpi *, S. Valente [1]

Department of Structural and Geotechnical Engineering, Politecnico di Torino, Corso Duca degli Abruzzi 24, 10129 Torino, Italy

Received 24 March 2003; received in revised form 12 December 2003

Abstract

The paper analyses the behaviour of concrete in the case of quasi-static fracture. The attention is focused on the interaction between strain-softening and time-dependent behaviour: a viscous rheological element (based on a fractional order rate law) is coupled with a micromechanical model for the fracture process zone. This approach makes it possible to include a whole range of dissipative mechanisms in a single rheological element. Creep fracture in mode I conditions is analysed through the finite element method and the cohesive (or fictitious) crack model. The comparison with creep tests executed on three-point bending conditions (three different load levels) shows a good agreement both in terms of failure-lifetime, and, load–displacement.

Keywords: Cohesive; Concrete; Crack; Creep; Fracture; Fractional; Long-term behaviour; Softening; Viscosity

1. Introduction

The long-term performance of concrete structures is fundamentally affected by the behaviour of the material after cracking. It is well known that concrete presents a diffused damage zone within which microcracking increases and stresses decrease as the overall deformation increases. This results in the softening of the material in the so called *fracture process zone* (FPZ), whose size can be compared with a characteristic dimension of the structure. This dimension is not constant and can vary during the evolutionary process. In this context, a numerical method (based on finite or boundary elements) has to be used together with the *cohesive* or *fictitious* crack model as shown by Barenblatt (1959), Dugdale (1960) and Hillerborg et al. (1976).

The interaction between strain-softening and time-dependent behaviour is analysed, with the emphasis on very slow or quasi-static fracture. This is the case of cracking in massive concrete structures like dams, where inertial forces can be neglected. In this field three approaches will be considered. The first is based on

* Corresponding author. Tel.: +39-11-5644886; fax: +39-11-5644899.
E-mail addresses: fabrizio.barpi@polito.it (F. Barpi), silvio.valente@polito.it (S. Valente).
[1] Tel.: +39-11-5644853; fax: +39-11-5644899.

0020-7683/$ - see front matter © 2004 Elsevier Ltd. All rights reserved.
doi:10.1016/j.ijsolstr.2003.12.025

Nomenclature

ε, ε_1	deformations of the rheological model
σ	stress of the rheological model, stress in the cohesive zone
σ_1	stress of the rheological model
E_1, E_2	Young's moduli of the rheological model
η	classical Newton's viscosity parameter
$\tau_1 = \frac{\eta}{E_1}$	relaxation time
$D^\alpha(\bullet) = \frac{\mathrm{d}^\alpha(\bullet)}{\mathrm{d}t^\alpha}$	fractional derivative operator of order α
α	order of differentiation
Γ	Euler's Gamma function $\left(\Gamma(x) = \int_0^\infty \mathrm{e}^i t^{(x-1)}\,\mathrm{d}t = \lim_{n\to\infty} \frac{n^x n!}{x(x+1)\cdots(x+n)}\right)$
$y(t)$	generic function of time
$\Phi_{1-\alpha}(t)$	kernel of the non-integer differentiation definition
$b_i(\alpha)$	ith coefficient of the numerical approximation of the non-integer derivative
E_c	concrete Young's modulus
K_1, K_2	elastic constants of the rheological model (see Fig. 6)
v	Poisson's ratio
$\mathscr{G}_F$	fracture energy (area below the curve of Fig. 5)
f_t	ultimate tensile strength
$\sigma_{F.C.T}$	maximum principal (tensile) stress acting at the fictitious crack tip
w	crack opening displacement (also called COD)
COD	crack opening displacement (also called w)
w_c	critical crack opening displacement (beyond w_c no stresses are transferred in the cohesive zone)
V_f	aggregate volume fraction
K_{Ic}^{hom}	fracture toughness of the homogenized material
β	concrete microstructural parameter $\left(\beta = \frac{(K_{Ic}^{hom})^2}{E_c(1-V_f)f_t}\right)$
$\Delta\sigma$	stress relaxation due to creep
Δw	creep displacement
t	time
z	distance measured from the bottom of the specimen
Δt	time step
$\mathrm{d}\sigma_t$	stress relaxation computed in each point of the FPZ (depends on local conditions only because it is assumed $w = \text{const}$)
$\mathrm{d}w_t$	creep displacement computed in each point of the FPZ (depends on local conditions only because it is assumed $\sigma = \text{const}$)
$\mathrm{d}\sigma$	real stress increment in the FPZ (depends on global and local conditions)
$\mathrm{d}w$	real displacement increment (depends on global and local conditions)
H	specimen height
P_{max}	maximum (or peak) load
P_{cost}	constant load level during the creep phase
$\boldsymbol{K}_T$	positive definite tangential stiffness matrix
$\boldsymbol{C}_T$	negative definite tangential stiffness matrix
$\boldsymbol{P}$	external load vector
$\Delta\lambda$	load multiplier
$\boldsymbol{Q}$	unbalanced load vector
$\Delta\boldsymbol{u}$	displacement vector

the concept of activation energy and rate-dependent softening that has been developed in a series of paper by Bazant and co-workers (Bažant, 1992; Bažant and Gettu, 1992; Bažant and Jiràsek, 1992, 1993; Wu and Bažant, 1993). This method was recently modified by van Zijl et al. (2001). The second approach is based on the inclusion of a standard rheological model for creep and relaxation into the fictitious crack model in order to accommodate the time dependency of crack opening, the latter in some instances being established by fitting stress relaxation results (Hansen, 1990, 1991; Zhou and Hillerborg, 1992; Zhang and Karihaloo, 1992a,b; Carpinteri et al., 1995, 1997; Barpi et al., 1999a). The third approach combines a micromechanical model for the static softening behaviour of cracked concrete in the fracture process zone (Huang and Li, 1989) with a rheological model for the time-dependent concrete behaviour (Santhikumar and Karihaloo, 1996, 1998; Santhikumar et al., 1998).

In the present paper the third approach is enhanced using a *fractional order rate* law and is applied to the numerical simulation of the three-point bending tests described by Zhou (1992).

2. Description of the rheological model

Rheology is concerned with time-dependent deformation of solids. In the simplest rheological model of the linear standard viscoelastic solid (Fig. 1), the springs are characterized by linear stress–displacement relationships:

$$\sigma_1 = E_1(\varepsilon - \varepsilon_1), \tag{1a}$$

$$\sigma_2 = E_2\varepsilon. \tag{1b}$$

In this paper, the dashpot is based on the following *fractional order rate* law for the internal variable ε_1:

$$D^{\alpha}\varepsilon_1 = \frac{\mathrm{d}^{\alpha}\varepsilon_1}{\mathrm{d}t^{\alpha}} = \frac{\sigma_1}{E_1\tau_1^{\alpha}} = \frac{\varepsilon - \varepsilon_1}{\tau_1^{\alpha}} \quad \text{with } \alpha \in (0,1), \tag{2}$$

where the fractional differentiation of a function $y(t)$ is defined according to Oldham and Spanier (1974) and Carpinteri and Mainardi (1997). Eq. (2) represents a generalization of the well-known Newton's constitutive law for the dashpot ($\sigma = \eta\frac{\mathrm{d}\varepsilon}{\mathrm{d}t}$).

In particular

$$D^{-(1-\alpha)}y(t) = \int_0^t \Phi_{1-\alpha}(t-\bar{t})y(\bar{t})\,\mathrm{d}\bar{t}, \tag{3}$$

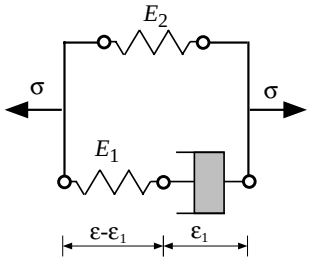

Fig. 1. Rheological model.

where

$$\Phi_{1-\alpha}(t) = \frac{t_+^{-\alpha}}{\Gamma(1-\alpha)} \quad \text{with } t_+ = \begin{cases} t & \text{if } t > 0 \\ 0 & \text{if } t < 0 \end{cases}. \tag{4}$$

In the previous expression Γ represents the *Gamma function*. Eq. (3) can also be obtained by using an hereditary model based on a Rabotnov fractional exponential kernel (see Karihaloo, 1995).

A convergent expression for the α-order fractional derivative operator D^{α} is given by

$$D^{\alpha}y(t) = D^{1}D^{-(1-\alpha)}y(t) = \frac{\mathrm{d}}{\mathrm{d}t}\int_0^t \Phi_{1-\alpha}(t-\bar{t})y(\bar{t})\,\mathrm{d}\bar{t} = \frac{1}{\Gamma(1-\alpha)}\frac{\mathrm{d}}{\mathrm{d}t}\int_0^t \frac{y(\bar{t})}{(t-\bar{t})^{-\alpha}}\,\mathrm{d}\bar{t}. \tag{5}$$

In the case of $\alpha = 1$ the classical dashpot with an integer order rate law is obtained from Eq. (2). In particular, the solutions for the relaxation problem (under constant w) and for the creep problem (under constant σ) become of exponential type, with τ_1 as the *relaxation time*, and $\tau_1 \frac{E_1+E_2}{E_2}$ as the *retardation time*. Response diagrams are plotted in Figs. 2 and 3 (see Barpi and Valente, 2003).

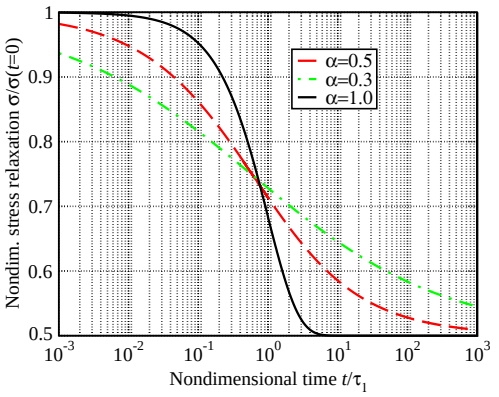

Fig. 2. Stress relaxation functions.

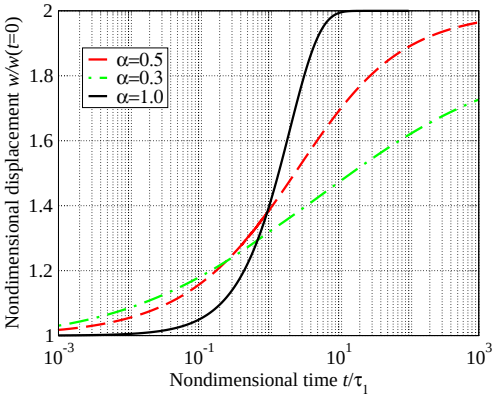

Fig. 3. Creep displacement functions.

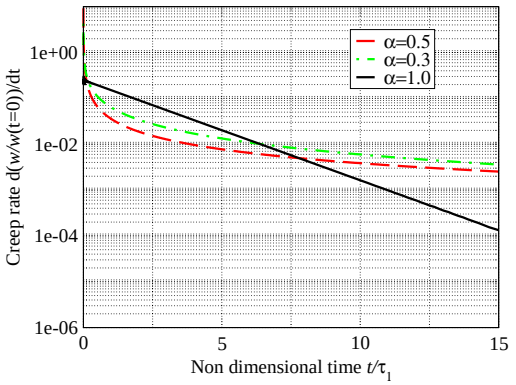

Fig. 4. Rate of creep displacement functions.

Fig. 4 shows the the influence of the non-integer derivative on the creep rate (i.e., the derivative with respect to time of the creep functions). This figure represents another way to show the difference between the model based on integer derivative (straight line) and the model based on a non-integer derivative (dashed and dashed-dotted curves).

2.1. Numerical integration of constitutive response

A possible approximation for the fractional differentiation of a function $y(t)$ is (Oldham and Spanier, 1974)

$$^{n+1}(D^{\alpha}y) = \frac{1}{(\Delta t)^{\alpha}} \sum_{j=0}^{n} b_j(\alpha)\, {}^{n+1-j}y, \tag{6}$$

where it is assumed that the spacing in time is uniform, i.e., ${}^{n}y = y(n\Delta t)$. The coefficients $b_j(\alpha)$ depend on the Gamma function as follows:

$$b_j(\alpha) = \frac{\Gamma(j-\alpha)}{\Gamma(-\alpha)\Gamma(j+1)}. \tag{7}$$

By using the recursion formula

$$\frac{\Gamma(j-\alpha)}{\Gamma(j+1)} = \frac{(j-1-\alpha)}{j}\,\frac{\Gamma(j-1-\alpha)}{\Gamma(j)}, \tag{8}$$

it is possible to avoid the evaluation of the Gamma function; the coefficients $b_j(\alpha)$ are given by

$$b_0(\alpha) = 1,\ \ldots,\ b_k(\alpha) = \frac{(k-1-\alpha)}{k} b_{k-1}(\alpha), \ldots \quad k = 1, \ldots, n. \tag{9}$$

For convenience, the expression in Eq. (6) can be rewritten as

$$^{n+1}(D^{\alpha}y) = \frac{1}{(\Delta t)^{\alpha}}({}^{n+1}y - {}^{n}\bar{y}), \tag{10}$$

where

$${}^{n}\bar{y} = -\sum_{j=1}^{n} b_j(\alpha)\, {}^{n+1-j}y \tag{11}$$

is a known quantity at time t_{n+1}.

At this point the updated stress quantities ${}^{n+1}\sigma$ can be obtained by using Eq. (10) with reference to Eq. (2). This *finite difference* approximation is applied to Eq. (2), and integrated over time, using the *General Midpoint Rule* (Enelund et al., 1999).

3. Description of the micromechanical model for the process zone

In each point of the fictitious process zone a micromechanical approach to tension softening is combined with rheological model described above, according to a strategy proposed in Santhikumar and Karihaloo (1996) and Santhikumar et al. (1998). Tension softening behaviour appears when the damage in the material has localized along eventual fracture planes. This behaviour has been successfully modeled using two- and three-dimensional micromechanical models (Huang and Li, 1989; Karihaloo, 1995).

All models provide a relationship between the residual tensile stress carrying capacity and crack opening displacement (COD) as a function of known concrete microstructural parameters (included in the factor β), e.g. aggregate volume fraction V_f, Young's modulus E_c, ultimate tensile strength f_t and fracture toughness of the homogenized material K_{Ic}^{hom} (see Fig. 5). According to these models, the function is assumed to be

$$\frac{w}{w_c} = \frac{(K_{Ic}^{hom})^2}{E_c(1-V_f)f_t}\frac{f_t}{\sigma}\left[1-\left(\frac{\sigma}{f_t}\right)^3\right] = \beta\frac{f_t}{\sigma}\left[1-\left(\frac{\sigma}{f_t}\right)^3\right]. \tag{12}$$

4. Rheological and micromechanical model interaction

During the loading phase each point of the FPZ moves on the same (σ–w) curve. Later on this condition does not hold any longer, due to the combined effect of *viscosity* and *damage*.

In order to understand how the rheological and micromechanical models interact, three simple cases are analysed:

1. if the displacement discontinuity w is kept constant along time step Δt, a stress relaxation $\Delta\sigma$ occurs according to the standard viscoelastic element described;
2. if the stress σ is kept constant along time step Δt, a creep displacement Δw occurs according to the standard viscoelastic element described;

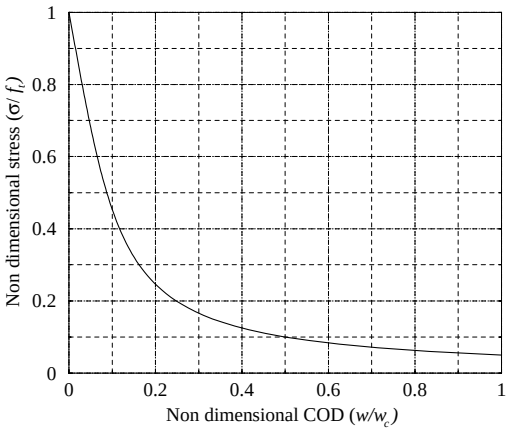

Fig. 5. Cohesive stress–COD law ($\beta = 0.05$).

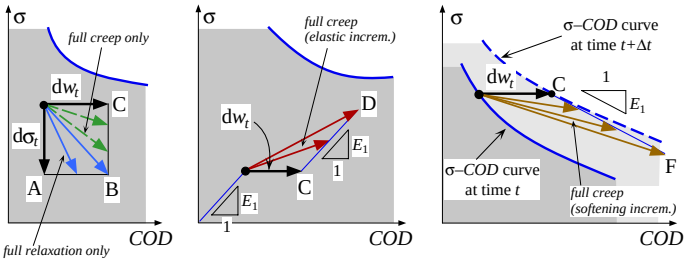

Fig. 6. Stress and displacement increments under constant load.

3. if both stress σ and displacement discontinuity w (also called COD) are forced to stay on the static curve (Eq. (12)), one of the two increments occurs as predicted by the rheological element, while the other is equal or smaller.

In greater detail, for the first case the unloading stiffness is assumed (effective spring hypothesis, Fig. 6, centre) while, for the second case, the stiffness tangent to the $(\sigma$–$w)$ curve of Eq. (12) is taken into account ($E_1 = |\frac{d\sigma}{dw}|$, Fig. 6, right).

At the end of each time step, the microcrack pattern changes and, in either case, stiffness is reduced. It is worth noting that each point follows a different path and, hence, exhibits a different stiffness, while $E_1 = E_2$ and τ_1 is constant. Finally, if both stress and displacement are prescribed, a creep increment of β induces a change in the $(\sigma$–$w)$ curve, as shown in Fig. 6.

In the case of integer order rate law, the related diagrams are published in Santhikumar and Karihaloo (1996) and Santhikumar et al. (1998).

5. Finite element analysis

In the present work, the continuum surrounding the process zone is assumed as *linear elastic*. All non-linear and time-dependent phenomena are assumed to occur in the *process zone*. When the fictitious crack tip advances by a pre-defined length, each point located on the crack trajectory, is split into two points. The virtual mechanical entity, acting on these two points only, is called *cohesive element*: the local behaviour of such an element follows the rules mentioned in the previous section. Each cohesive element interacts with the others only through the undamaged continuum, external to the process zone.

According to the finite element method, by taking the unknowns to be the n nodal displacement increments, $\Delta\boldsymbol{u}$, and assuming that compatibility and equilibrium conditions are satisfied at all points in the solid, the following system of n equations with $n+1$ unknowns ($\Delta\boldsymbol{u}$, $\Delta\lambda$ or Δt) is obtained. The creep effect is incorporated by simply adding the pseudo-load induced by relaxation to the load vector in the equilibrium equations (Bocca et al., 1991; Barpi et al., 1999a):

$$(\boldsymbol{K}_{\mathrm{T}} + \boldsymbol{C}_{\mathrm{T}})\Delta\boldsymbol{u} = \Delta\lambda\boldsymbol{P} + \Delta t\boldsymbol{Q}, \tag{13}$$

where

- $\boldsymbol{K}_{\mathrm{T}}$: positive definite tangential stiffness matrix, containing contributions from linear elastic (undamaged) elements and possible contributions from cohesive elements having (σ, w) below the curve of Fig. 5. The conditions in which this possibility applies will be described later on;
- $\boldsymbol{C}_{\mathrm{T}}$: negative definite tangential stiffness matrix, containing contributions from cohesive elements with (σ, w) on the curve of Fig. 5;

- $\boldsymbol{P}$: the vector of external load;
- $\Delta\lambda$: maximum load multiplier which is compatible with Eq. (12) and the fictitious crack tip growth condition ($\sigma_{\mathrm{F.C.T}} = f_{\mathrm{t}}$);
- $\boldsymbol{Q}$: vector of unbalanced load (or pseudo-load) due to relaxation in the process zone, related to a unitary time increment.

During the loading phase the behaviour of the process zone is assumed to be time-independent ($\boldsymbol{Q} = \boldsymbol{0}$), the external load changes ($\Delta\lambda \neq 0$, and $\Delta t = 0$) while, during the sustained loading phase, is assumed to be time-dependent ($\boldsymbol{Q} \neq \boldsymbol{0}$) and the external load is kept constant ($\Delta\lambda = 0$, and $\Delta t \neq 0$).

5.1. Interaction between cohesive elements

During the loading phase, all the stress paths in the FPZ are forced to follow the (σ–w) law (see Eq. (12)). For the boundary condition analysed dw is *always* and *everywhere* positive. A more complex situation occurs during the next loading phase (*sustained*): the unloading stiffness approaches ∞ when w tends to 0^+. In order to avoid this difficulty, a threshold value has to be assumed for w. A cohesive element is classified as *active*, and submitted to the rheological model, when and only when its w is bigger than the threshold, assumed equal to 0.001 w_{c}. Otherwise the stress path is forced to follow the (σ–w) law as it occurs during the loading phase.

According to the rheological model, for each active cohesive element, it is possible to compute the stress relaxation under constant w (dσ_{t}) as well as the creep displacement under constant σ(dw_{t}). It is important to notice that dσ_{t} and dw_{t} are *threshold values* computed according to the micromechanical model, while dσ and dw are *real values* obtained from equilibrium and compatibility conditions.

The compatibility conditions can be grouped in the following cases:

1. full relaxation only: $\mathrm{d}\sigma = \mathrm{d}\sigma_{\mathrm{t}} < 0$ and $\mathrm{d}w < \mathrm{d}w_{\mathrm{t}}$ (see segment AB in Fig. 6);
2. full creep only: $\mathrm{d}\sigma < \mathrm{d}\sigma_{\mathrm{t}} < 0$ and $\mathrm{d}w = \mathrm{d}w_{\mathrm{t}}$ (see segment BC in Fig. 6);
3. full creep with elastic increment: $\mathrm{d}\sigma = (\mathrm{d}w - \mathrm{d}w_{\mathrm{t}})E_1 > 0$ and $E_1 > 0$ and $\mathrm{d}w > \mathrm{d}w_{\mathrm{t}}$ (see segment CD in Fig. 6);
4. full creep with softening increment: $\mathrm{d}\sigma = (\mathrm{d}w - \mathrm{d}w_{\mathrm{t}})E_1 < 0$ and $E_1 < 0$ and $\mathrm{d}w > \mathrm{d}w_{\mathrm{t}}$ (see segment CF in Fig. 6).

In this context, the *Helmholtz free energy* is assumed as the objective function to be minimised at each time step under the constraints shown in Fig. 6. The use of optimisation techniques in structural analysis to solve the variational inequality that occurs in elastoplasticity is well known (see Maier, 1971). Since the loading conditions are assumed as piecewise linear, each *physical* time step is divided into numerous *logical* substeps that can be solved through the *Simplex method*, a classical linear programming tool. When case (3) or case (4) are applied, stiffness matrix coefficients are changed from one substep to the next (Bocca et al., 1991; Barpi et al., 1999a). Otherwise they are kept constant during all the substep iterations. In order to follow this process of classification, an inner loop must be introduced.

Creep rupture time is reached when the smallest eigenvalue of the tangential stiffness matrix becomes negative: this means that the external load can no longer be kept constant.

6. Comparison between experimental and numerical results

The experimental tests, executed on pre-notched beams, described by Zhou (1992), were simulated numerically. The experimental procedure is based on two phases. In the first, the external load grows from

Table 1
Material properties

E (GPa)	ν (–)	$\mathcal{G}_f$ (N/m)	f_t (MPa)
36	0.10	82	2.8

Table 2
Numerical parameters

w_c (mm)	τ_1 (s)	$\Delta t/\tau_1$ (–)	β (–)	Element size (mm)
0.22	150	1/50	0.05	0.0625

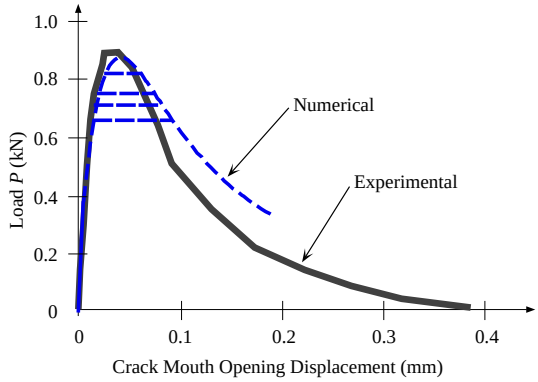

Fig. 7. Experimental and numerical load vs. crack mouth opening displacement.

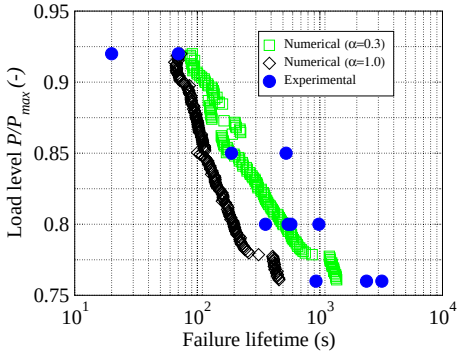

Fig. 8. Comparison between experimental and numerical results.

zero to the nominal level (a fraction of the maximum load P_{max}) under deflection control (5×10^{-6} m/s), while, during the second, the load is kept constant until the creep rupture occurs (*pre-peak* sustained bending).

These tests are usually associated with the name of *pre-peak sustained bending* tests. Of course, in order to know the maximum load $P_{max} \approx 900$ N, a number of static tests have to be previously executed. To

overcome this difficulty, different investigators prefer to use the so-called *post-peak* tests where the creep phase starts beyond the peak point (Carpinteri et al., 1997; Barpi et al., 1999b). The specimen dimensions are $10\times10\times80$ cm, the notch depth is 5 cm, while the material properties, as described in Zhou (1992), are presented in Table 1.

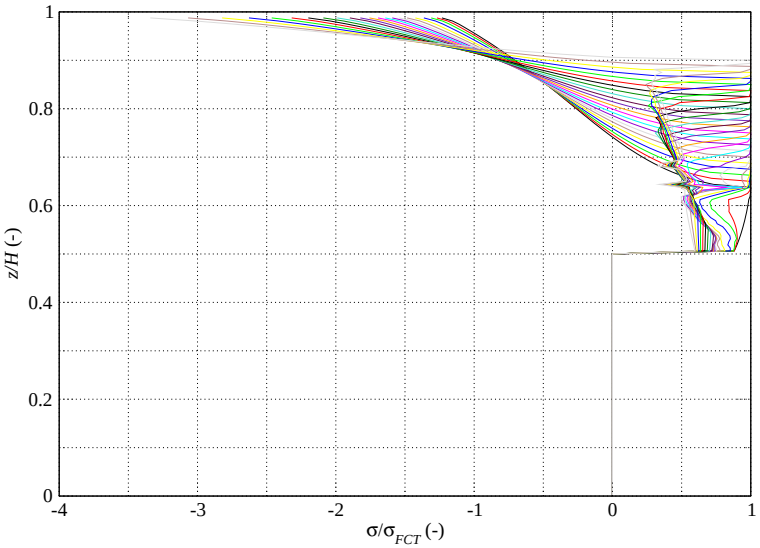

Fig. 9. Stress distribution in the fracture zone for the case $\frac{P_{\text{cost}}}{P_{\max}} = 0.76$.

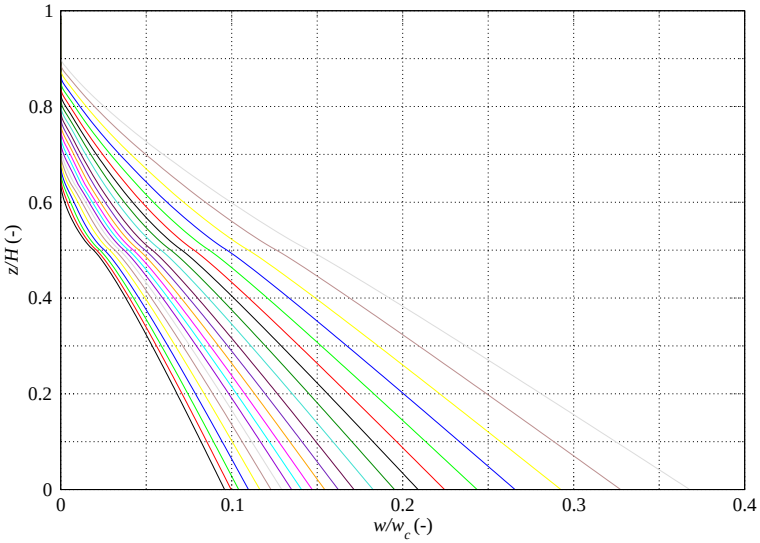

Fig. 10. Crack opening distribution in the fracture zone for the case $\frac{P_{\text{cost}}}{P_{\max}} = 0.76$.

The numerical simulations were executed using the values listed in Table 2, and neglecting the time-dependent behaviour of the undamaged material. As suggested in Barpi et al. (1999a) the following limit is applied to each step: $|\frac{d\sigma}{f_t}| \leqslant 0.01$.

Fig. 7 shows the experimental and numerical load vs. crack mouth opening displacement curves for static tests as well as for sustained load tests. Fig. 8 shows the load level vs. the logarithm of the failure-lifetime

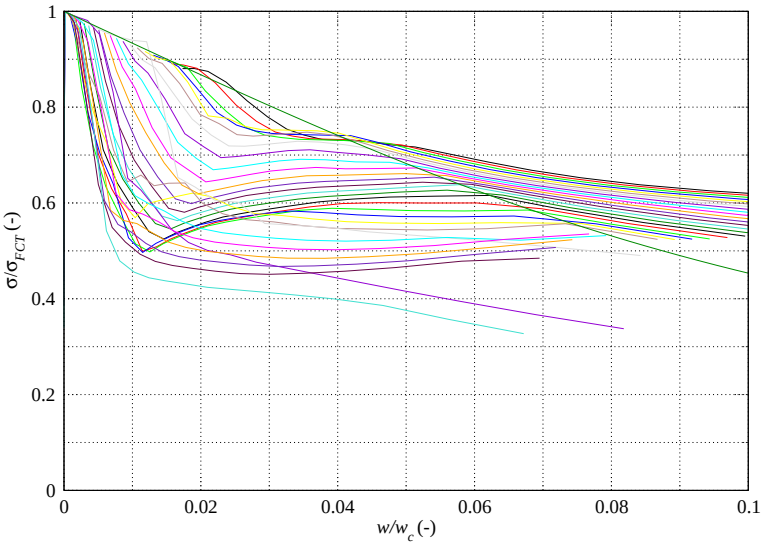

Fig. 11. Stress paths for the case $\frac{P_{cost}}{P_{max}} = 0.76$.

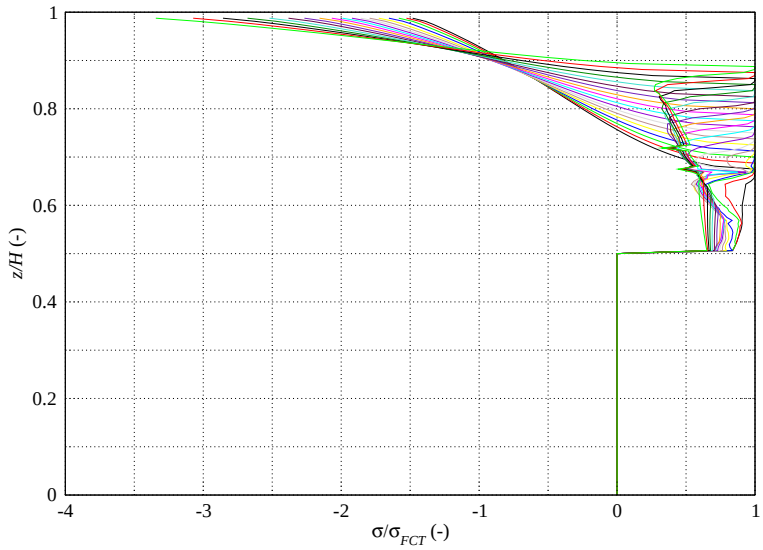

Fig. 12. Stress distribution in the fracture zone for the case $\frac{P_{cost}}{P_{max}} = 0.85$.

(creep rupture time), for different values of the fractional derivative order α (0.30 and 1.00). The best fitting of the experimental results is achieved assuming $\alpha = 0.30$. Experimental and numerical results appear to be in good agreement.

Figs. 9, 12 and 15 show the non-dimensional stress $(\sigma/\sigma_{\mathrm{F.C.T}})$ distribution in the fracture zone for the cases $\frac{P_{\mathrm{cost}}}{P_{\max}} = 0.76$, 0.85, 0.92. The maximum value of tensile stress is f_{t}, according to the cohesive model.

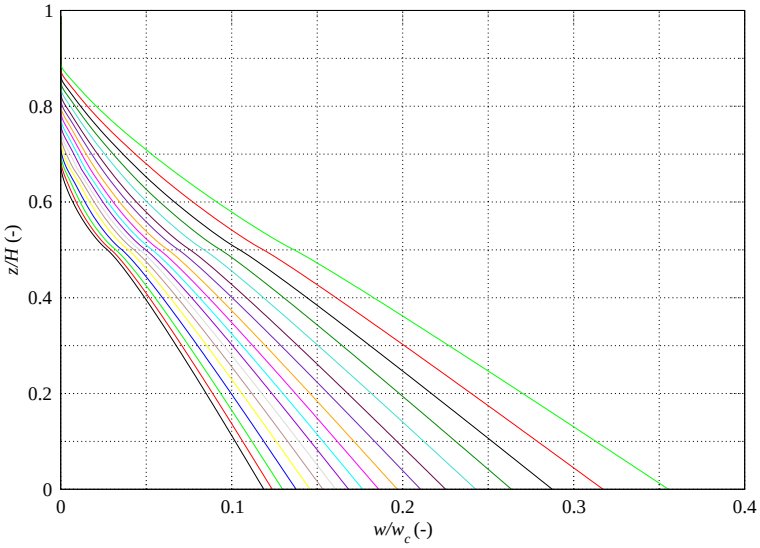

Fig. 13. Crack opening distribution in the fracture zone for the case $\frac{P_{\mathrm{cost}}}{P_{\max}} = 0.85$.

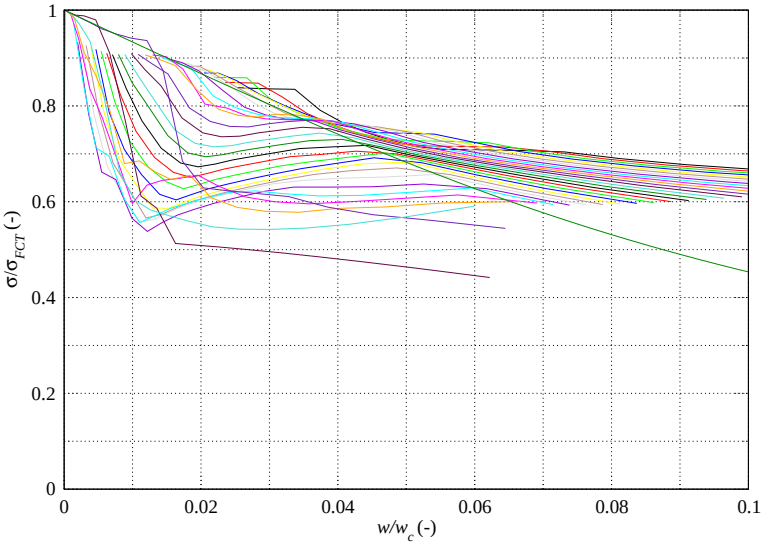

Fig. 14. Stress paths for the case $\frac{P_{\mathrm{cost}}}{P_{\max}} = 0.85$.

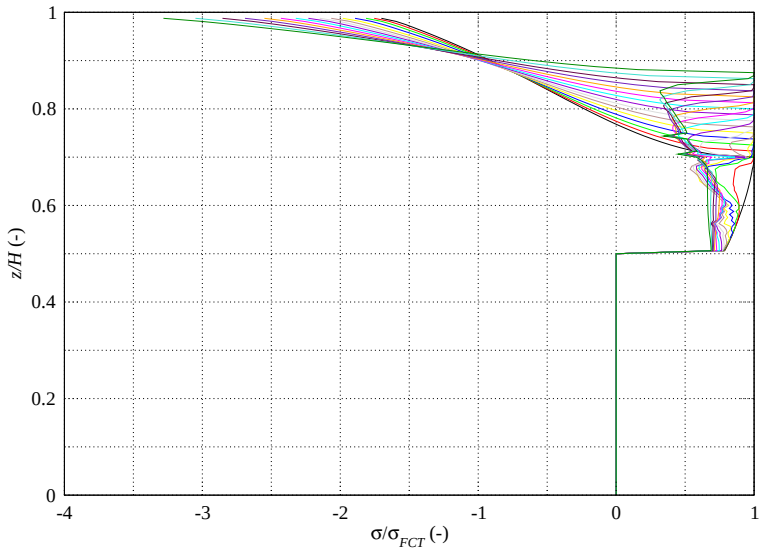

Fig. 15. Stress distribution in the fracture zone for the case $\frac{P_{\text{cost.}}}{P_{\max}} = 0.92$.

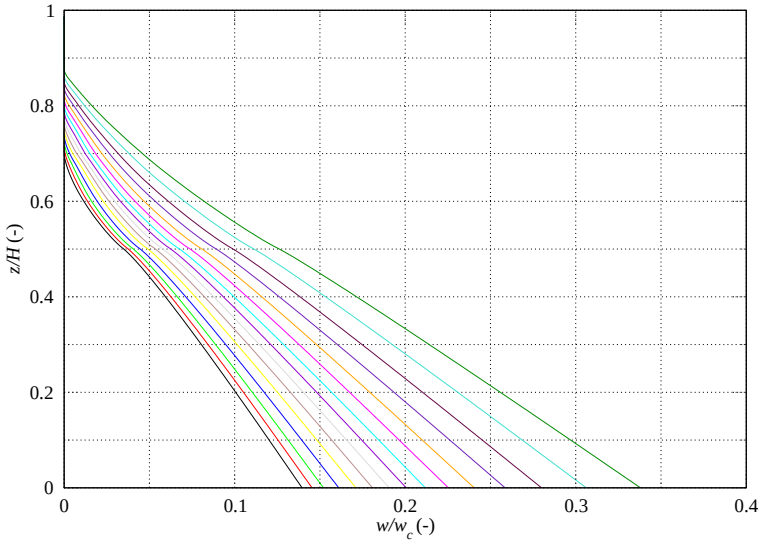

Fig. 16. Crack opening distribution in the fracture zone for the case $\frac{P_{\text{cost.}}}{P_{\max}} = 0.92$.

Figs. 10, 13 and 16 show the non-dimensional opening (w/w_c) distribution in the fracture zone for the same cases. Finally, Figs. 11, 14 and 17 show the stress paths, followed from some cohesive elements during the external load growth, for the three cases examined. As explained before, the couples $(\sigma$–$w)$ are not restricted to stay on the static envelope.

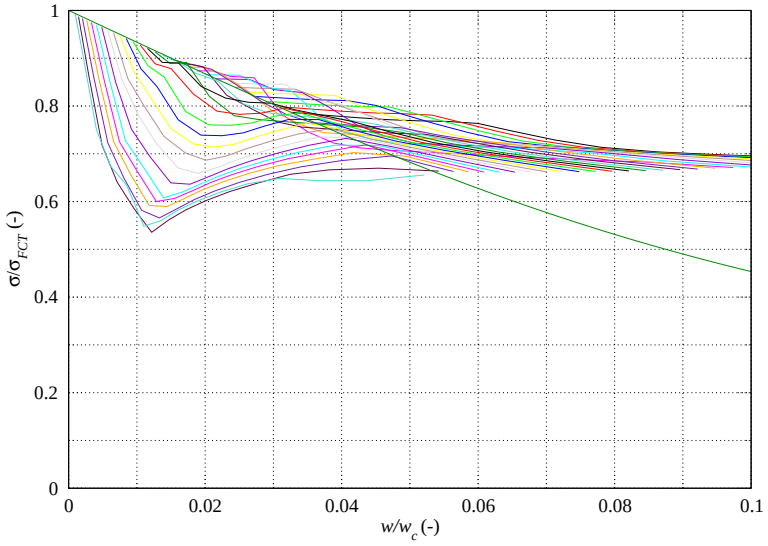

Fig. 17. Stress paths for the case $\frac{P_{\text{cost}}}{P_{\max}} = 0.92$.

7. Conclusions

- The interaction between *strain-softening* and *time-dependent* behaviour of uncracked material can be analysed through the *micromechanical* model presented.
- The incremental problem is formulated as *linear with threshold*. In the FPZ the equilibrium, compatibility and minimum *Helmholtz free energy* conditions are applied.
- Each *physical* time step is divided into numerous *logical* substeps that are solved through the *Simplex method*, a classical linear programming tool.
- A *single* rheological has been used. It has been shown that *four material properties only*, namely, the elastic moduli E_1 and E_2, the relaxation time τ_1 and the order α of the fractional derivative are needed to describe the phenomenon. Hence, a *fractional order rate* makes it possible to include a *whole spectrum* of dissipative mechanisms in a *single* viscous element.
- It is *not necessary* to use long chains of rheological elements, whose properties are difficult to determine.

Acknowledgements

The financial support provided by the Italian Department of Education, University and Scientific Research (MIUR) to the research project on "*Dam-reservoir-foundation systems: dynamic, diagnostic and safety analyses*" (grant number 2002087915_006) is gratefully acknowledged.

References

Barenblatt, G.I., 1959. The formation of equilibrium cracks during brittle fracture: general ideas and hypotheses. Journal of Applied Mathematics and Mechanics, pp. 622–636.

Barpi, F., Valente, S., 2003. Creep and fracture in concrete: a fractional order rate approach. Engineering Fracture Mechanics 70, 611–623.

Barpi, F., Chillè, F., Imperato, L., Valente, S., 1999a. Creep induced cohesive crack propagation in mixed mode. In: Durban, D., Pearson, J.R.A. (Eds.), Non-Linear Singularities in Deformation and Flow. Kluwer Academic Publishers, The Netherlands, pp. 155–168.

Barpi, F., Ferrara, G., Imperato, L., Valente, S., 1999b. Lifetime of concrete dam models under constant loads. Materials and Structures 32, 103–111.

Bažant, Z.P., 1992. Rate effects, size effects and nonlocal concepts for fracture of concrete and other quasi-brittle materials. In: Shah, S. (Ed.), Mechanisms of Quasi-brittle Materials. Kluwer, Dordrecht, pp. 131–153.

Bažant, Z.P., Gettu, R., 1992. Rate effects and load relaxation in static fracture of concrete. American Concrete Institute Journal 89 (5), 456–468.

Bažant, Z.P., Jiràsek, M., 1992. *R*-curve modeling of rate effects in static fracture and its interference with size effects. In: Bažant, Z.P. (Ed.), Fracture Mechanics of Concrete Structures. Elsevier, London, pp. 918–923.

Bažant, Z.P., Jiràsek, M., 1993. *R*-curve modeling of rate and size-effects in quasibrittle fracture. International Journal of Fracture 62, 355–373.

Bocca, P., Carpinteri, A., Valente, S., 1991. Mixed-mode fracture of concrete. International Journal of Solids and Structures 27, 1139–1153.

Carpinteri, A., Mainardi, F., 1997. Fractals and Fractional Calculus in Continuum Mechanics. Springer, Wien.

Carpinteri, A., Valente, S., Zhou, F.P., Ferrara, G., Melchiorri, G., 1995. Crack propagation in concrete specimens subjected to sustained loads. In: Wittmann, F.H. (Ed.), Fracture Mechanics of Concrete Structures. Aedificatio, Germany, pp. 1315–1328.

Carpinteri, A., Valente, S., Zhou, F.P., Ferrara, G., Melchiorri, G., 1997. Tensile and flexural creep rupture tests on partially-damaged concrete specimens. Materials and Structures 30, 269–276.

Dugdale, D.S., 1960. Yielding of steel sheets containing slits. Journal of Mechanics and Physics of Solids 8, 100–114.

Enelund, M., Mähler, L., Runesson, K., Lennart Josefson, B., 1999. Formulation and integration of the standard linear viscoelastic solid with fractional order rate laws. International Journal of Solids and Structures 36, 2417–2442.

Hansen, E.A., 1990. A visco-elastic fictitious crack model. In: Shah, S., Swartz, S., Wang, M. (Eds.), Micromechanics of Quasi-brittle Materials. Elsevier, London, pp. 156–165.

Hansen, E.A., 1991. Influence of sustained load on the fracture zone of concrete. In: van Mier, J.G.M., Rots, J.G., Bakker, A. (Eds.), Fracture Processes in Concrete Rock and Ceramics. E&FN Spon, pp. 829–838.

Hillerborg, A., Modeer, M., Petersson, P.E., 1976. Analysis of crack formation and crack growth in concrete by means of fracture mechanics and finite elements. Cement and Concrete Research 6, 773–782.

Huang, J., Li, V., 1989. A meso-mechanical model of the tensile behaviour of concrete. Composites 20, 370–378.

Karihaloo, B.L., 1995. Fracture Mechanics and Structural Concrete. Longman Scientific and Technical, England.

Maier, G., 1971. Incremental plastic analysis in the presence of large displacements and physical instabilizing effects. International Journal of Solids and Structures 7, 345–372.

Oldham, K.B., Spanier, J., 1974. The Fractional Calculus. Academic Press, New York.

Santhikumar, S., Karihaloo, B.L., 1996. Time-dependent tension softening. Mechanics of Cohesive-Frictional Materials 1, 295–304.

Santhikumar, S., Karihaloo, B.L., 1998. Time dependent behaviour of cracked and ageing concrete. In: de Borst, R., Bićanić, N., Mang, H., Meschke, G. (Eds.), Computational Modelling for Concrete Structures. Balkema, Rotterdam, The Netherlands, pp. 455–465.

Santhikumar, S., Karihaloo, B.L., Reid, G., 1998. A model for ageing visco-elastic tension softening material. Mechanics of Cohesive-Frictional Materials 3, 27–39.

van Zijl, G., de Borst, R., Rots, J., 2001. The role of crack rate dependence in the long-term behaviour of cementitious materials. International Journal of Solids and Structures 38, 5063–5092.

Wu, Z.S., Bažant, Z.P., 1993. Finite element modeling of rate effects in concrete with influence of creep. In: Bažant, Z.P., Carol, I. (Eds.), Creep and Shrinkage of Concrete. E&FN Spon, London, pp. 427–432.

Zhang, C., Karihaloo, B., 1992a. Stability of a crack in a large concrete dam. In: C.E. Trans. Inst. Engrs. Aust. (CE34), pp. 369–375.

Zhang, C., Karihaloo, B., 1992b. Stability of a crack in linear visco-elastic tension softening material. In: Bažant, Z.P. (Ed.), Fracture Mechanics of Concrete Structures. Elsevier, London, pp. 75–81.

Zhou, F.P., 1992. Time-dependent crack growth and fracture in concrete. PhD thesis, Report TVBM-1011, Lund University of Technology, Sweden.

Zhou, F.P., Hillerborg, A., 1992. Time-dependent fracture of concrete: testing and modelling. In: Bažant, Z.P. (Ed.), Fracture Mechanics of Concrete Structures. Elsevier Applied Science, The Netherlands, pp. 906–911.